Nonperturbative calculation of projectile-electron loss, target ionization, and capture in $He^+ + Ne$ collisions

Tom Kirchner and Marko Horbatsch
Department of Physics and Astronomy, York University, Toronto, Ontario, Canada M3J 1P3
(Received 1 December 2000; published 16 May 2001)

The $He^+ + Ne$ collision system, in which the projectile electron as well as the target electrons undergo inelastic transitions is investigated in the independent-particle model with a time-dependent screening potential. We use the basis generator method to solve the single-particle equations for all electrons and combine the transition probabilities statistically to calculate charge-state correlated and more inclusive total cross sections in the energy range of 10 to 1000 keV/amu. Good agreement with available experimental data is found except for the lowest projectile energies, where it is indicated that a more refined dynamical screening model is required. We demonstrate the importance of Pauli blocking for the electron transfer to the dressed projectile and discuss the role of the electron-electron interaction between projectile and target electrons, which is not included in our model.

DOI: 10.1103/PhysRevA.63.062718 PACS number(s): 34.50.Fa, 34.70.+e

I. INTRODUCTION

Ion-atom collisions with active electrons on projectile and target have attracted considerable attention in recent years. In particular, the excitation and ionization of dressed projectiles in collisions with neutral noble gas atoms or hydrogen molecules have been investigated experimentally and theoretically in some detail (for recent reviews see, e.g., Refs. [1–3]). These studies were motivated in part by the idea that the transition of the projectile electron can be induced either by an interaction with the target nucleus or by an interaction with one of the target electrons, and that both processes have different signatures that should make it possible to distinguish them. This picture is based on a perturbative description of the scattering process [3]. To first order, the simultaneous excitation or ionization of the projectile electron and one of the target electrons can only be induced by the electron-electron interaction. On the other hand, an inelastic transition of the projectile electron alone (with the target remaining in its ground state) is due to the combined Coulomb potentials of the target nucleus and the target electrons. The latter process has been called the screening mode, since the target electrons only participate by screening the nucleus. In this way, they reduce the transition probabilities of the projectile electron when compared to a collision with a bare target nucleus. By contrast, the direct excitation or ionization of both centers due to the electron-electron interaction has been referred to as antiscreening. We will use the terms antiscreening and electron-electron process as synonyms in the present paper.

Clear evidence for the operation of both mechanisms has been found in numerous experiments, first through total cross section measurements [4] and more recently by measuring the momentum distributions of the recoil ions, which are very different in both processes [5].

On the theoretical side, the application of perturbative methods to the problem at hand has a rather long tradition dating back to the works of Bates and Griffing in the 1950s [6]. While a first-order treatment appears to be sufficient to describe the electron-electron process over a rather broad range of kinematical situations [1,7–9], it has been recognized that a reliable calculation of the screening contribution requires nonperturbative models when target atoms heavier than helium are considered. This is due to the fact that the total cross sections are dominated by contributions from small impact parameters, where the screened target potential becomes too strong to allow a first- or second-order treatment. Under such circumstances the antiscreening mode is less important, as simultaneous transitions of the projectile electron and one or several target electrons can also be mediated by independent single-particle interactions [1].

Although detailed cross section measurements were performed for dressed projectiles colliding with heavier noble gas atoms (see, e.g., Refs. [10–13] and references therein) only few theoretical efforts to describe and explain these data have been reported in the literature. Apart from applications of the relatively simple free-collision model (also referred to as classical impulse approximation) [13,14] nonperturbative methods to calculate the (dominant) screening contribution to the ionization of dressed projectiles have been reported only recently [9,15,16]. These calculations were restricted to impact energies above 250 keV/amu, since they involved the assumption that electron transfer between the centers is neglible. Moreover, it was not attempted to calculate the target ionization as well, thus leaving a large body of experimental data for charge-state correlated cross sections over a wide range of impact energies virtually unexplained. The present work is intended as a step to fill this void.

We consider the $He^+ + Ne$ collision system in the energy range from 10 to 1000 keV/amu. Our treatment is based on the independent-particle model (IPM), in which the transitions of all active electrons are governed by effective single-particle Hamiltonians. Recently, we studied the validity of this approach for bare-ion collisions with neon, argon, and oxygen atoms [17–21] over a broad range of impact energies. We found that a large number of single- and double-electron processes can be successfully calculated, when the many-electron target atom is described in terms of a single-particle potential that accounts accurately for electronic exchange effects. Moreover, we developed a (relatively) simple model to account for time-dependent screening effects and demonstrated that the results for multiple-electron transitions

can be significantly improved in such a dynamical screening model [21]. Important ingredients of these works have been the development and implementation of the basis generator method (BGM) to propagate the effective single-particle equations [22,23], and the issue of how to extract probabilities for multiple-electron transitions from the single-particle solutions. This has been discussed for the cases of multiple-electron loss and ionization in Ref. [18] and more generally for charge-state correlated processes and excitations in Ref. [20].

In the present paper we extend these techniques to the problem under consideration, in which the projectile carries into the collision an electron that can be ionized or captured by the same token as the target electrons. The paper is organized as follows. In Sec. II A the time-dependent many-electron problem is formulated in the IPM and the approximations used for the effective single-particle potentials are discussed. The adaption of the BGM to the present collision system is briefly explained in Sec. II B. Section III is devoted to the issue of how to extract probabilities for measurable cross sections from the BGM solutions. The single-particle probabilities of interest and probabilities for global processes are defined in Sec. III A, while the calculation of charge-state correlated cross sections is explained in Sec. III B. In Sec. IV we discuss our results in comparison with experimental data. The discussion is split into three parts. We begin with the cross sections for the total production of recoiling target ions and free electrons in Sec. IV A. In Sec. IV B we present results for electron capture and projectile-electron loss cross sections, in which the final charge state of the target is not determined. Charge-state correlated data are discussed in Sec. IV C. In Sec. V our findings are summarized and directions of future work are pointed out.

II. THEORETICAL DESCRIPTION OF THE $(N+1)$-ELECTRON SCATTERING SYSTEM

We consider the collision between an ion carrying one electron and an N-electron closed-shell target atom. When relativistic effects can be neglected the $(N+1)$-electron system is described by the Hamiltonian (we use atomic units, i.e., $\hbar=m_e=e=1$)

$$\hat{H}(t)=\sum_{i=1}^{N+1}\left(-\frac{1}{2}\Delta_i-\frac{Q_T}{r_{iT}}-\frac{Q_P}{r_{iP}}\right)+\sum_{i<j}^{N+1}\frac{1}{r_{ij}}. \qquad (1)$$

Here, Q_T and Q_P are the charges of the target and projectile nuclei, respectively. The distances of the ith electron to the target and projectile centers are measured by r_{iT} and r_{iP}, while the distance between two of the $N+1$ electrons is denoted by r_{ij}. When the nuclear motion is described by a classical straight-line trajectory the set of coordinates $\{r_{iT}\}$ or the set $\{r_{iP}\}$ (or both) are functions of time depending on the choice of the reference frame.

Before the collision the projectile and target subsystems are well separated, and the $(N+1)$-electron wave function is given as an (antisymmetrized) product of the ground-state wave functions of both centers. If the target ground state is described in terms of an effective single-particle picture (e.g., the Hartree Fock model or approximations thereof) the $(N+1)$-particle initial state reduces to a single Slater determinant $|\psi_{1\sigma_1}\cdots\psi_{N\sigma_N}\phi_\sigma\rangle$, in which the spin orbitals $|\psi_{i\sigma_i}\rangle$ denote the occupied target states and $|\phi_\sigma\rangle$ the occupied projectile state with the spin indices $\sigma_i=\uparrow,\downarrow$. We note that a single Slater determinant is in general not sufficient to describe the initial state when the target atom is of open-shell nature. This situation has been discussed, e.g., for $He^+ + He^+$ collisions, in which different spin configurations have been taken into account [24]. Simple product or single Slater determinant initial states constitute the usual starting point for perturbative calculations of ionization from the projectile [3]. Although the electron-electron interaction among the target electrons has been approximated by an effective single-particle potential at this point, the Hamiltonian still contains the two-particle interaction between the target electrons and the projectile electron. It is this two-particle potential that enables the simultaneous transition of a target electron and the projectile electron in first-order perturbation theory (antiscreening).

A. *IPM* description with time-dependent target potential

In the following, we approximate the electron-electron interaction by effective single-particle potentials, thus neglecting the antiscreening mechanism. We explain our model on the basis of the time-dependent Hartree Fock (TDHF) approach to clarify the approximations involved and to indicate possible improvements. The TDHF approach starts from the assumption that the wave function of the electronic system can be characterized as a single Slater determinant for all times, i.e., throughout the collision. The TDHF equations are obtained by variation of the action functional involving the Hamiltonian (1) with this constraint [25]. For the $(N+1)$-electron problem under consideration they can be written in the form

$$\begin{aligned} i\partial_t\psi_{i\sigma_i}(\mathbf{r},t)=&\left(-\frac{1}{2}\Delta-\frac{Q_T}{r_T}-\frac{Q_P}{r_P}\right.\\ &\left.+\sum_{k=1}^{N}\int d^3r'\frac{|\psi_{k\sigma_k}(\mathbf{r}',t)|^2}{|\mathbf{r}-\mathbf{r}'|}\right)\psi_{i\sigma_i}(\mathbf{r},t)\\ &-\sum_{k=1}^{N}\delta_{\sigma_i\sigma_k}\int d^3r'\frac{\psi^*_{k\sigma_k}(\mathbf{r}',t)\psi_{i\sigma_i}(\mathbf{r}',t)}{|\mathbf{r}-\mathbf{r}'|}\\ &\times\psi_{k\sigma_k}(\mathbf{r},t)+\int d^3r'\frac{|\phi_\sigma(\mathbf{r}',t)|^2}{|\mathbf{r}-\mathbf{r}'|}\psi_{i\sigma_i}(\mathbf{r},t)\\ &-\delta_{\sigma_i\sigma}\int d^3r'\frac{\phi^*_\sigma(\mathbf{r}',t)\psi_{i\sigma_i}(\mathbf{r}',t)}{|\mathbf{r}-\mathbf{r}'|}\phi_\sigma(\mathbf{r},t),\\ &i=1,\ldots,N, \qquad (2)\end{aligned}$$

$$i\partial_t \phi_\sigma(\mathbf{r},t) = \left(-\frac{1}{2}\Delta - \frac{Q_P}{r_P} - \frac{Q_T}{r_T} + \sum_{k=1}^{N} \int d^3r' \frac{|\psi_{k\sigma_k}(\mathbf{r}',t)|^2}{|\mathbf{r}-\mathbf{r}'|} \right) \phi_\sigma(\mathbf{r},t) - \sum_{k=1}^{N} \delta_{\sigma\sigma_k} \int d^3r' \frac{\psi^*_{k\sigma_k}(\mathbf{r}',t)\phi_\sigma(\mathbf{r}',t)}{|\mathbf{r}-\mathbf{r}'|} \psi_{k\sigma_k}(\mathbf{r},t), \tag{3}$$

where in general $r_T = |\mathbf{r} - \mathbf{R}_T(t)|$ and $r_P = |\mathbf{r} - \mathbf{R}_P(t)|$ with $\mathbf{R}_T(t)$ and $\mathbf{R}_P(t)$ defining the classical motion of the nuclei. Equation (2) describes the time propagation of the initially occupied target orbitals in the combined potentials of the nuclei and the effective electron-electron interaction. We are distinguishing between the direct (Hartree) and exchange terms due to the target electrons and due to the projectile electron, since they are treated differently in the following. Likewise, Eq. (3) describes the propagation of the single electron initially bound to the projectile. We now introduce further approximations to facilitate the treatment.

(1) We neglect the two-center exchange terms that couple the target electrons with the projectile electron in the case of parallel-spin directions. As a consequence, the time development of the spin-up and spin-down electrons of the target is identical in this approximation. As long as ionization is considered this should be no severe restriction, but one may expect that the omission of the exchange terms is more crucial in the case of capture. Furthermore, we note that the orthogonality between the propagated target states and the propagated projectile state (normally ensured in the TDHF method) is lost, since the single-particle Hamiltonians that govern their time development become different when the two-center exchange terms are neglected.

(2) We assume that the remaining exchange term in Eq. (2) can be described by a local, i.e., multiplicative single-particle potential v_x^ψ acting on the propagated orbitals. The single-particle equations (2) and (3) can then be summarized as

$$i\partial_t \psi_i(\mathbf{r},t) = \hat{h}_\psi(t)\psi_i(\mathbf{r},t) \quad i = 1, \ldots, N, \tag{4}$$

$$i\partial_t \phi(\mathbf{r},t) = \hat{h}_\phi(t)\phi(\mathbf{r},t), \tag{5}$$

with the Hamiltonians

$$\hat{h}_\psi(t) = -\frac{1}{2}\Delta - \frac{Q_T}{r_T} - \frac{Q_P}{r_P} + v_{ee}^\psi(\mathbf{r},t) + v_H^\phi(\mathbf{r},t), \tag{6}$$

$$\hat{h}_\phi(t) = -\frac{1}{2}\Delta - \frac{Q_P}{r_P} - \frac{Q_T}{r_T} + v_H^\psi(\mathbf{r},t), \tag{7}$$

and the single-particle potentials

$$v_{ee}^\psi(\mathbf{r},t) = v_H^\psi(\mathbf{r},t) + v_x^\psi(\mathbf{r},t) \tag{8}$$

$$v_H^\psi(\mathbf{r},t) = \sum_{k=1}^{N} \int d^3r' \frac{|\psi_k(\mathbf{r}',t)|^2}{|\mathbf{r}-\mathbf{r}'|} \tag{9}$$

$$v_H^\phi(\mathbf{r},t) = \int d^3r' \frac{|\phi(\mathbf{r}',t)|^2}{|\mathbf{r}-\mathbf{r}'|}. \tag{10}$$

The spin indices have been omitted, since all terms are now spin independent. Note that the single-particle equations (4) and (5) are still coupled via the time-dependent Hartree potentials (9) and (10).

In analogy to our previous work on bare-ion collisions with many-electron target atoms [21] we decompose the single-particle potentials (8) to (10) into contributions that account for electronic screening and exchange in the initial state and contributions due to time-dependent variations during the collision process

$$v_{ee}^\psi(\mathbf{r},t) = v_{ee}^T(r_T) + \delta v_{ee}^\psi(\mathbf{r},t) = v_H^T(r_T) + v_x^T(r_T) + \delta v_H^\psi(\mathbf{r},t) + \delta v_x^\psi(\mathbf{r},t), \tag{11}$$

$$v_H^\phi(\mathbf{r},t) = v_H^P(r_P) + \delta v_H^\phi(\mathbf{r},t). \tag{12}$$

The potential v_{ee}^T of the undisturbed electronic system at the target is obtained from the exchange-only version of the optimized potential method (OPM) [26]. In this model, exchange effects are described by a multiplicative single-particle potential v_x^T that cancels the self-interaction contribution contained in the Hartree potential v_H^T exactly. The ground-state Hartree potential v_H^P of the projectile ion is obtained by inserting a hydrogen-like $1s$-orbital into Eq. (10)

$$v_H^P(r_P) = \frac{1}{r_P}[1 - (1 + Q_P r_P)\exp(-2Q_P r_P)]. \tag{13}$$

In the *no-response* approximation defined by

$$\delta v_{ee}^\psi(\mathbf{r},t) = \delta v_H^\psi(\mathbf{r},t) = \delta v_H^\phi(\mathbf{r},t) = 0 \tag{14}$$

the single-particle Hamiltonians (6) and (7) reduce to

$$\hat{h}_T(t) = -\frac{1}{2}\Delta + \left(-\frac{Q_T}{r_T} + v_{ee}^T(r_T) \right) + \left(-\frac{Q_P}{r_P} + v_H^P(r_P) \right), \tag{15}$$

$$\hat{h}_P(t) = -\frac{1}{2}\Delta - \frac{Q_P}{r_P} + \left(-\frac{Q_T}{r_T} + v_H^T(r_T) \right). \tag{16}$$

The grouping of potentials in Eqs. (15) and (16) allows a simple interpretation: The target electrons are propagated in the atomic ground-state potential and the moving Coulomb potential of the projectile that is screened by the electrostatic potential due to the (frozen) $1s$ electron. The projectile electron is propagated in the Coulomb potential of the He^{2+} nucleus and the Coulombic target potential screened by the ground-state Hartree component of the effective electron-electron interaction. Note that the potentials v_{ee}^T in Eq. (15)

and v_H^T in Eq. (16) are obtained from the same set of self-consistently determined ground-state orbitals of the target atom.

Our previous investigations demonstrated that the *no-response* approximation is justified when the relative velocity of the nuclear motion is large compared to typical orbital velocities of the active electrons. In this kinematic region the electron density does not change considerably during the (short) interaction with the projectile. At low to intermediate impact energies time-dependent screening effects gain importance, in particular when multiple-electron processes are considered. For the present study we have included these effects on the level of the model proposed in Ref. [21]. This model was designed to account in a global fashion for the increasing attraction of the atomic target potential as ionization and capture set in during the collision. It involves the assumption that the dynamical target potential can be represented by a linear combination of ionic ground-state potentials weighted with the time-dependent probabilities to create the corresponding charge states q during the collision. Furthermore, the ionic potentials were expressed as sums of the Coulomb potential of the nucleus and the effective potential v_{ee}^T for the electron-electron interaction of the neutral atom scaled to yield the desired asymptotic behavior for each charge state q. With these assumptions we arrived at the following expression for the response potential at the target [21]

$$\delta v_{ee}^{\psi}(\mathbf{r},t) \approx \delta v_{ee}^{\psi}(r_T,t) = -\frac{P_{\rm loss}^T(t) + P_0^{\rm loss}(t) - 1}{N-1} v_{ee}^T(r_T). \tag{17}$$

$P_{\rm loss}^T$ denotes the net electron loss from the target, i.e., the average number of removed electrons, and $P_0^{\rm loss}$ is the probability that no electrons are removed. $P_0^{\rm loss}$ is calculated from $P_{\rm loss}^T$ according to the binomial formula

$$P_0^{\rm loss}(t) = \left(1 - \frac{P_{\rm loss}^T(t)}{N}\right)^N. \tag{18}$$

The net electron loss from the target $P_{\rm loss}^T$ in turn is obtained from a channel representation of the propagated orbitals $\psi_i(t)$ in each time step

$$P_{\rm loss}^T(t) = N - \sum_{i=1}^{N} \sum_{v=1}^{V} |\langle \varphi_v^T | \psi_i(t) \rangle|^2, \tag{19}$$

where the set $\{|\varphi_v^T\rangle, v = 1 \cdots V\}$ contains all bound target states populated noticeably in the collision process.

In Ref. [21] we emphasized that the use of undisturbed atomic eigenstates as channel functions $|\varphi_v^T\rangle$ leads to fluctuating transition probabilities after the collision, if a response potential $\delta v_{ee}^{\psi}(t)$ is included in the Hamiltonian. This problem was encountered in several TDHF calculations [27] and is associated with the nonlinearity of the Hamiltonian. For the present model of dynamical screening all transition amplitudes become stable when the analysis at the target center is based on parametrically time-dependent eigenfunctions $|\varphi_v^T(t)\rangle$ of the Hamiltonian that includes the response potential [21]

$$|\varphi_v^T\rangle \equiv |\varphi_v^T(t)\rangle \quad v = 1, \ldots, V \tag{20}$$

$$\left(-\frac{1}{2}\Delta - \frac{Q_T}{r_T} + v_{ee}^T(r_T) + \delta v_{ee}^{\psi}(r_T,t)\right) |\varphi_v^T(t)\rangle = \varepsilon_v(t) |\varphi_v^T(t)\rangle. \tag{21}$$

The functions $|\varphi_v^T(t)\rangle$ correspond to the average (fractional) charge state of the target atom after the collision and are thus consistent with the used mean-field description.

The inclusion of $\delta v_{ee}^{\psi}(t)$ in the Hamiltonian (15) accounts only for one aspect of dynamical screening effects. Clearly, an increase in the attraction of the target atom during the collision also influences the behavior of the projectile electron. Mathematically this effect corresponds to unfreezing the effective Hartree potential v_H^T in Eq. (16). Similarly, the dynamical behavior of the projectile electron induces a variation of v_H^P in Eq. (15). It seems feasible to include these effects on the same level as in Eq. (17), but such an extension involves a considerable complication in the solution of the single-particle equations, since both sets [Eqs. (4) and (5)] would be coupled during the propagation. This issue is beyond the scope of the present paper and is deferred to a future work. Note that the coupling is avoided in the response model that includes only $\delta v_{ee}^{\psi}(t)$.

B. Solution of the single-particle equations

The single-particle equations are solved in the *no-response* approximation (14) and the dynamical screening model defined by Eq. (17) by separate BGM calculations for the active target and projectile electrons. Since we assume the nuclei to move on straight-line trajectories, we can choose the origin of the reference frame in both calculations differently. For the active neon orbitals [Eq. (4)] we choose the target center and use the same expansion as in our previous investigation of $He^{2+} + Ne$ collisions [21]

$$|\psi_i(t)\rangle = \sum_{\mu=0}^{M_T} \sum_{v=1}^{V_T} d_{\mu v}^{Ti}(t) |\chi_v^{\mu}(t)\rangle, \tag{22}$$

$$|\chi_v^{\mu}(t)\rangle = [W_P(t)]^{\mu} |\varphi_v^T\rangle \quad \mu = 0, \ldots, M_T, \tag{23}$$

$$W_P(t) = \frac{1}{r_P}(1 - \exp(-r_P)). \tag{24}$$

In the target frame the projectile moves along the trajectory $\mathbf{R}(t) = (b, 0, vt)$ with impact parameter b and constant velocity v. Therefore, W_P depends on time, via $r_P = |\mathbf{r_T} - \mathbf{R}(t)|$. The basis includes all undisturbed target states $|\varphi_v^T\rangle$ of the $KLMN$ shells calculated numerically on a fine mesh and 100 functions from the set $\{|\chi_v^{\mu}(t)\rangle, \mu \geq 1\}$ up to order $\mu = M_T = 8$. We note that we use the same basis for the *no-response* calculation [Eq. (14)] and the calculation with the time-dependent screening potential (17).

To solve Eq. (5) for the Hamiltonian (16) we choose the projectile center as the origin of the reference frame and expand the active orbital according to

$$|\phi(t)\rangle=\sum_{\mu=0}^{M_P}\sum_{v=1}^{V_P} d_{\mu v}^{P}(t)|\tilde{\chi}_v^{\mu}(t)\rangle, \tag{25}$$

$$|\tilde{\chi}_v^{\mu}(t)\rangle=[W_T(t)]^{\mu}|\varphi_v^{P}\rangle \quad \mu=0,\ldots,M_P, \tag{26}$$

$$W_T(t)=\frac{1}{r_T}(1-\exp(-r_T)). \tag{27}$$

In this frame, the neon center moves along the straight line $\mathbf{R}(t)=(b,0,vt)$ with constant velocity v, and the distance r_T depends on time via $r_T=|\mathbf{r_P}-\mathbf{R(t)}|$. The basis set of Eqs. (25) and (26) includes all hydrogen-like eigenfunctions $|\varphi_v^P\rangle$ of the $KLMN$ shells of the He^+ ion and 95 functions of the set $\{|\tilde{\chi}_v^{\mu}(t)\rangle,\mu\geqslant 1\}$ up to order $\mu=M_P=8$. The choice was guided by calculating the correlation diagram of the (frozen) quasimolecular system $(HeNe)^+$ in the basis [22].

We note that in both basis sets the BGM states of higher order are constructed with powers of purely Coulombic potentials, which are regulated to avoid divergent matrix elements and to improve the representation of bound states on the other center [Eqs. (24) and (27)]. We did not build the BGM hierarchy with powers of the screened potentials that are present in the Hamiltonians [cf. Eqs. (15) and (16)]. This choice was found to be more efficient in generating states, which account properly for the electron-transfer contribution of the time-propagated orbitals in a number of test cases [28].

III. ANALYSIS OF IONIZATION AND TRANSFER PROCESSES

A. Single-electron and net transition probabilities

The statistical evaluation of probabilities for the various charge-changing processes is based on the calculated single-particle probabilities for ionization, and attachment to the target and projectile nuclei for all propagated orbitals. These probabilities are obtained by projecting the solutions of the time-dependent single-particle equations onto states, which characterize the processes considered and are consistent with the boundary conditions for asymptotic times ($t_f\rightarrow\infty$) in order to ensure stable results. In practice, it proved to be sufficient to stop the propagation at times t_f, which correspond to an internuclear separation of 45 a.u.

For the active target electrons we define the single-particle probabilities for attachment to the target and the projectile as

$$p_i^{T\rightarrow T}=\sum_{v=1}^{V_T}|\langle\varphi_v^T(t_f)|\psi_i(t_f)\rangle|^2 \tag{28}$$

$$p_i^{T\rightarrow P}=\sum_{k=1}^{K_P}|\langle\varphi_k^P(t_f)|\psi_i(t_f)\rangle|^2. \tag{29}$$

The channel functions at the target $|\varphi_v^T(t_f)\rangle$ are the eigenfunctions of the asymptotic target Hamiltonian that includes the response potential [Eq. (21)] and are obtained by diagonalizing this Hamiltonian in the BGM basis [21]. The asymptotic Hamiltonian of the isolated projectile system contains the Coulomb potential and the screening potential due to the bound $1s$ electron [cf. Eq. (15)]. Therefore, the channel functions $|\varphi_k^P(t_f)\rangle$ are chosen as (moving) eigenstates of this Hamiltonian and are calculated numerically. We have chosen K_P to include all states of the KLM shells. With the assumption that the summations in Eqs. (28) and (29) cover the bound parts with sufficient accuracy the single-particle probabilities for transitions to the continuum are obtained from the requirement

$$p_i^{T\rightarrow C}=1-p_i^{T\rightarrow T}-p_i^{T\rightarrow P}. \tag{30}$$

Similarly, the single-particle probabilities for the active projectile electron are defined as

$$p^{P\rightarrow P}=\sum_{v=1}^{V_P}|\langle\varphi_v^P|\phi(t_f)\rangle|^2, \tag{31}$$

$$p^{P\rightarrow T}=\sum_{k=1}^{K_T}|\langle\varphi_k^0(t_f)|\phi(t_f)\rangle|^2, \tag{32}$$

$$p_i^{T\rightarrow C}=1-p_i^{P\rightarrow P}-p_i^{P\rightarrow T}. \tag{33}$$

The states $|\varphi_v^P\rangle$ are the hydrogen-like eigenfunctions of the projectile and are explicitly included in the basis [Eq. (26)]. The channel functions for transfer to the target $|\varphi_k^0(t_f)\rangle$ are again chosen as eigenstates of the corresponding asymptotic Hamiltonian obtained from Eq. (16). These states are consistent with the boundary condition for capture and ensure asymptotic stability. However, they are rather artificial from a physical point of view, since they correspond to an exponentially decaying potential (note that the Hartree potential v_H^T decreases as N/r_T asymptotically, and thus compensates the nuclear potential for a neutral atom $N=Q_T$). In fact, we found only two bound eigenstates for this potential with energies $\varepsilon_{1s}=-26.60$ a.u. and $\varepsilon_{2s}=-0.306$ a.u. compared to the eigenenergies of the full target potential $-Q_T/r_T+v_{ee}^T$ (including exchange) $\varepsilon_{\mathrm{Ne}(1s)}^{\mathrm{OPM}}=-30.82$ a.u., $\varepsilon_{\mathrm{Ne}(2s)}^{\mathrm{OPM}}=-1.718$ a.u. This unphysical situation is a consequence of the *no-response* approximation for the effective Hartree potential v_H^{ψ} [cf. Eqs. (7) and (14)]. From a practical point of view it does not cause significant problems for the calculation of global and charge-state correlated cross sections, as long as one considers intermediate to high impact energy collisions, where the electron transfer from the projectile to the target is small. However, one can expect that the transfer is significantly underestimated at low energies, as transitions to $Ne(2p)$ states, which are impossible in our model are likely to become important. This assumption is based on the fact that we found large-transition probabilities for the inverse process, in which a $Ne(2p)$ electron is captured to the K shell of the projectile.

It has been argued that the transfer from the projectile to the target is physically blocked by the Pauli principle and that the inability to account for this fact has to be regarded as a problem in the IPM [9]. We note that this is only partly true, since the Pauli principle does not exclude capture processes that occur simultaneously with target ionization or capture into vacant excited states. These processes could be analyzed in a well defined and meaningful way for full TDHF calculations, which guarantee the orthogonality between the propagated target and projectile states through the formalism of *inclusive probabilities* [29]. Our work on the projection problem suggests that full TDHF calculations should be analyzed with respect to eigenstates of the corresponding time-dependent mean-field Hamiltonian [cf. Eq. (21)] rather than using eigenstates of the static asymptotic Hamiltonians. It can be expected that the time-dependent mean field at the target exhibits a Coulomb tail with fractional mean charge after the collision due to ionization events. As a consequence, the corresponding spectrum of bound eigenstates would be infinite and hence physically more meaningful than the present case, where only two bound eigenfunctions are found.

Summation of the single-particle probabilities Eqs. (28) to (33) yields the average number of electrons bound to target and projectile and released to the continuum

$$P_{\rm av}^{T}=\sum_{i=1}^{N} p_i^{T\to T}+p^{P\to T}\equiv P_{\rm net}^{T\to T}+p^{P\to T}, \tag{34}$$

$$P_{\rm av}^{P}=p^{P\to P}+\sum_{i=1}^{N} p_i^{T\to P}\equiv p^{P\to P}+P_{\rm net}^{T\to P}, \tag{35}$$

$$P_{\rm av}^{C}=\sum_{i=1}^{N} p_i^{T\to C}+p^{P\to C}=N+1-P_{\rm av}^{T}-P_{\rm av}^{P}. \tag{36}$$

Two global observables that have been measured in Refs. [10,11] can be directly calculated from these net probabilities; the total production of recoil ions (denoted by σ_+ in Ref. [10]) and the total production of free electrons (denoted by σ_- in Ref. [10]). The former corresponds to an integral over impact parameter of the probability

$$P_{+}=N-P_{\rm av}^{T}, \tag{37}$$

while the latter is obtained by integrating $P_{\rm av}^{C}$.

B. Multiple-electron transition probabilities

The calculation of more detailed cross sections, for which the final charge state of one or both centers is determined is based on statistical combinations of the single-particle probabilities (28) to (33). As a first step we calculate the probabilities P_{kl}^{T} for k-fold capture from the target to the projectile and simultaneous l-fold target ionization. This can be done by application of the shell-specific trinomial analysis [30] or, alternatively, by use of the analysis in terms of products of binomials [20]. The latter method was introduced to avoid nonzero probabilities for higher-order capture events, which occur in the trinomial analysis and lead to the unphysical production of negatively charged ions. The basic idea is to distribute the net capture probability $P_{\rm net}^{T\to P}$ [cf. Eq. (35)] over the physical capture channels by carrying out binomial statistics with the new single-particle probability $P_{\rm net}^{T\to P}/M$, in which M is the number of electrons that can be accommodated by the projectile. The desired probability P_{kl}^{T} is then obtained by multiplying the k-fold capture probability by an independent l-fold shell-specific binomial ionization probability

$$P_{kl}^{T}=P_{k}^{T\to P}P_{l}^{T\to C}, \tag{38}$$

$$P_{k}^{T\to P}=\frac{M!}{k!(M-k)!}\left(\frac{P_{\rm net}^{T\to P}}{M}\right)^{k}\left(1-\frac{P_{\rm net}^{T\to P}}{M}\right)^{M-k}, \tag{39}$$

$$P_{l}^{T\to C}=\sum_{l_1,\ldots,l_m=0;\ l_1+\cdots+l_m=l}^{N_1,\ldots,N_m}\prod_{i=1}^{m}\frac{N_i!}{l_i!(N_i-l_i)!}\times(p_i^{T\to C})^{l_i}(1-p_i^{T\to C})^{N_i-l_i}. \tag{40}$$

In Eq. (40), m is the number of initially occupied shells in the target atom and N_i is the number of electrons in each shell.

For the present case of He^+ + Ne collisions we chose $M=1$ to avoid the production of negative final projectile charge states. Strictly speaking this choice is too restrictive, since it prohibits the physically allowed process of double capture with simultaneous ionization of the projectile. However, the corresponding charge-state correlated cross section, where two electrons are found at the projectile and one in the continuum should be strongly dominated by single capture with simultaneous target ionization. As long as one does not attempt to distinguish both processes (e.g., by measuring the momentum distribution of the ionized electron), the restriction $M=1$ should not lead to significant errors.

The probabilities P_{kl}^{T} are then combined with the single-particle probabilities of the active projectile electron. In analogy to the set $\{P_{kl}^{T}\}$ we define

$$P_{00}^{P}=p^{P\to P}, \tag{41}$$

$$P_{10}^{P}=p^{P\to T}, \tag{42}$$

$$P_{01}^{P}=p^{P\to C} \tag{43}$$

and calculate the probability P_{mn} to find m electrons bound to the projectile and n electrons bound to the target after the collision according to

$$P_{mn}=\sum_{i,j=0,1;\ i+j\leqslant 1} P_{kl}^{T}P_{ij}^{P}, \quad m+n\leqslant N+1, \tag{44}$$

with

$$k=m+i+j-1, \tag{45}$$

$$l=N+i-n-k=N+1-m-n-j, \tag{46}$$

and the understanding that $P_{kl}=0$, if one of the indices lies outside the range $0\cdots N$. To illustrate the procedure we consider the probability for an event, where one electron is found in the continuum, while the projectile has not changed its charge state. From Eqs. (44) to (46) we obtain

$$P_{1,N-1}=P_{01}^{T}P_{00}^{P}+P_{10}^{T}P_{01}^{P}+P_{11}^{T}P_{10}^{P}. \tag{47}$$

The three terms in Eq. (47) correspond to different processes, which are not distinguished in an experiment, in which (only) the final charge states of projectile and target are measured in coincidence. The first term corresponds to pure single target ionization and certainly dominates the cross section considered. The second term describes the transfer of one electron from the target to the projectile with simultaneous ionization of the projectile, and the third term corresponds to single target ionization together with the exchange of two electrons between the centers.

More global processes, where only the charge state of one of the collision partners is determined are calculated by summation of the contributing probabilities P_{mn}. For the so-called total electron loss, where the projectile is stripped (i.e., $m=0$) this summation yields

$$P_{\mathrm{loss}}^{P}\equiv\sum_{n}\ P_{0n}=P_{0}^{T\rightarrow P}(P_{01}^{P}+P_{10}^{P}), \tag{48}$$

if the products-of-binomials analysis is used to calculate P_{kl}^{T} [Eqs. (38) to (40)]. This is simply the probability to lose the projectile electron multiplied by the probability not to capture a target electron. Similarly, one finds that the neutralization of the projectile ($m=2$) is given as the net capture probability $P_{\mathrm{net}}^{T\rightarrow P}$ multiplied by the probability P_{00}^{P} that the projectile electron is not removed with a slight imperfection caused by the products-of-binomials analysis, in which probability conservation is not exactly fulfilled [20].

It can be expected that the Pauli exclusion principle would be important for the projectile neutralization channel. Capture to the *K* shell of the projectile is only possible, when the spin direction of the captured electron opposes the spin of the projectile electron (assuming the latter remains in the ground state). This effect is ignored in the statistical analysis. It can be taken into account by using the formalism of *inclusive probabilities* [29]. This analysis starts from the assumption that the propagated many-electron state and the final states of interests are represented by single Slater determinants (for $N+1$ electrons in our case). The desired probability to find exactly *m* electrons at the projectile is then obtained as an ordered sum of determinants of the single-particle density matrix [31]. Since the analysis is based on antisymmetric wave functions, Pauli blocking is taken into account.

For the present collision system two interrelated problems arise as a consequence of the approximations. Firstly, the single-particle amplitudes for the population of bound-projectile states are calculated with respect to two different sets of functions [cf. Eqs. (29) and (31)]. In practice, this turned out to be a minor problem. We have projected the propagated target orbitals also onto the hydrogen-like projectile states used in Eq. (31) and found no significant deviations from the results of Eq. (29), where channel functions of the screened potential are used. Secondly, the formalism of *inclusive probabilities* makes use of the orthogonality of the propagated states to rewrite reduced density matrices as determinants of the single-particle density matrix [29]. As mentioned above, the orthogonality between the propagated target states and the propagated projectile state is not maintained during the collision in our approximation. Therefore, one has to check that the overlap between the propagated states is sufficiently small before applying the *inclusive probabilities* analysis. The nonorthogonality problem is largest for the propagated target $2p_1$ state at low projectile energies, where capture to the projectile is strong. At 10 keV/amu we found overlaps up to $|\langle\phi(t_f)|\psi_{2p_1}(t_f)\rangle|^2\approx 0.6$. The overlap decreases with increasing projectile energy and the sum $\Sigma_i|\langle\phi(t_f)|\psi_i(t_f)\rangle|^2$ does not exceed 0.2 for $E_P \geqslant 50$ keV/amu.

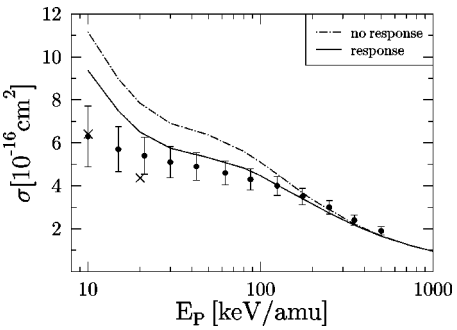

FIG. 1. Total cross section σ_+ for the net recoil ion production as a function of impact energy for $He^+ + Ne$ collisions. Theory: present calculations with and without inclusion of time-dependent screening denoted by the full curve and chain curve, respectively; the crosses denote the result of the modified calculation described in the text. Experiment: closed circles [10].

IV. RESULTS AND DISCUSSION

In this section we present results for the global cross sections discussed in Sec. III A and for more detailed processes, in which the final charge state of one or both centers are determined (cf. Sec. III B). Our calculations are based on the dynamical screening model defined by the potential (17). Only for the total production of recoil ions and the total production of free electrons do we compare them with the results of the *no response* approximation [Eq. (14)].

A. Net recoil ion and free electron production

We start the discussion of results with the total production of recoil ions σ_+ [cf. Eq. (37)] and the total production of free electrons σ_- [cf. Eq. (36)]. Our results for σ_+ obtained in the *no-response* approximation [Eq. (14)] and in the model that includes the time-dependent screening potential $\delta v_{ee}^{\psi}(t)$ of Eq. (17) are compared with the experimental data of Ref. [10] in Fig. 1.

At high-impact energies E_P both calculations give very similar results and show good agreement with experiment. This confirms the assumption that dynamical screening effects are unimportant when the relative velocity of the nuclei is large compared to the average velocity of the active electrons. We note that the same behavior was found for $He^{2+} + Ne$ collisions in Ref. [21]. For lower-impact energies the cross section of the model that includes $\delta v_{ee}^{\psi}(t)$ lies below

the *no-response* data indicating that the increased attraction of the target potential becomes more important as the projectile velocity decreases. The agreement with experiment is good down to $E_P = 20$ keV/amu, whereas the *no-response* results clearly lie outside the experimental error bars for $E_P < 100$ keV/amu.

For impact energies $E_P \leqslant 20$ keV/amu the cross sections of the calculation that includes time-dependent screening increase too rapidly compared with the experimental data. In this region, where the probabilities for electron loss from the target are large the *no-response* approximation used for the propagation of the projectile electron [Eq. (16)] is likely to be inadequate. Unfreezing the Hartree potential v_H^T in Eq. (16) would result in a total effective target potential with long-range Coulomb character. With such a potential the coupling between the initial projectile $1s$ state and bound-target states should increase significantly. As target electrons are removed with high probability the Pauli principle no longer prohibits electron transfer from the projectile to the target center. This process would reduce σ_+, since on average more electrons would be bound to the target after the collision.

To test this scenario on a qualitative level we performed a calculation, in which the frozen Hartree potential v_H^T in Eq. (16) was replaced by the effective potential v_{ee}^T that includes the attractive exchange component [Eq. (8)] and hence reduces the screening of the Coulomb potential of the nucleus. The total effective target potential exhibits a $-1/r_T$ tail in this model and corresponds roughly to a situation, in which one target electron is removed. We added the probability $p^{P\to T}$ calculated in this model to the unchanged probability $P_{\rm net}^{T\to T}$ according to Eq. (34) to calculate σ_+. The results of this procedure are included in Fig. 1 at 10 and 20 keV/amu. At 10 keV/amu the calculated cross section coincides with the measured data point, whereas it lies below experiment at 20 keV/amu. Obviously, the model is too crude to describe the energy dependence of the cross section, but it indicates that a more refined dynamical screening model, in which *all* effective potentials in the Hamiltonians (15) and (16) are unfrozen, could suffice to explain the experimental data at low impact energies.

The total free-electron production cross section σ_- is displayed in Fig. 2. This cross section corresponds to the sum of ionization from the projectile and the net ionization from the target [Eq. (36)]. According to our calculations 70–80 % of σ_- is due to the ionization of target electrons. The calculation that includes the response potential (17) leads to very good agreement with the experimental data of Ref. [11] down to $E_P = 10$ keV/amu, while the results of the *no-response* approximation are in closer agreement with the somewhat larger cross sections of Ref. [10] in the region of low to intermediate-impact energies. The discrepancy between the two experimental data sets was discussed in Ref. [11], and the more recent measurements were considered to be accurate, although no clear explanation for possible errors in the data of Ref. [10] was provided.

Free electrons are also produced by the interaction of a target electron with the projectile electron (antiscreening)

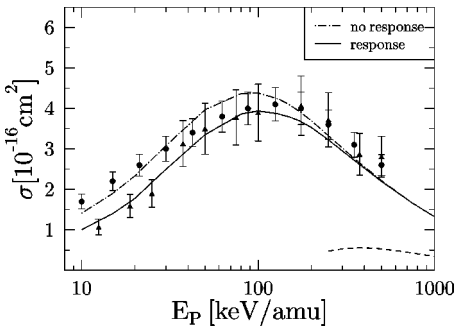

FIG. 2. Total cross section σ_- for free-electron production as a function of impact energy for $He^+ + Ne$ collisions. Theory: present calculations with and without inclusion of time-dependent screening denoted by the full curve and chain curve, respectively; dashed curve: PWBA calculation for the antiscreening mode [9] multiplied by a factor of 2. Experiment: closed circles [10]; closed triangles [11].

that is neglected in our model. Its contribution to ionization from the projectile was calculated in the plane-wave Born approximation (PWBA) with an improved summation over all target states [9] as described in Ref. [7]. The ionization of the projectile electron in the antiscreening mode is accompanied by the excitation or ionization of one of the target electrons. As ionization strongly dominates [2], two free electrons are produced in this process. Accordingly, we have included the PWBA results multiplied by a factor of 2 in Fig. 2. The cross section is rather flat as a function of impact energy. It has been argued that the electron-electron process exhibits a threshold, roughly determined by the condition $v^2/2 > I_P + I_T$, where I_P and I_T denote the ionization energies of the projectile and target electrons, respectively, [2,32]. With $I_P = 2$ a.u. and $I_T = 0.79$ a.u. [33] the threshold is situated at $E_{ts} \approx 140$ keV/amu corresponding to $v = 2.36$ a.u. for the present collision system. In fact, it can be observed in Fig. 2 that our results for σ_- lie below the experimental data for energies above this threshold. The agreement improves considerably when one adds the PWBA antiscreening cross section to our results. The PWBA is not extended down to threshold for two reasons: (1) the PWBA is inaccurate near threshold and (2) the threshold is not defined sharply due to the Compton profiles of the bound electrons.

B. Total electron capture and loss

In the following we restrict the discussion to calculations that include dynamical screening according to Eq. (17). First, we consider the total cross section for neutralization of the projectile, i.e., electron capture. Figure 3 shows results obtained from the trinomial analysis and the analysis in terms of products of binomials as described in Sec. III B along with experimental data. In the energy range from 10 to 100 keV/amu the trinomial results are smaller than the products-of-binomials cross sections. This is due to the fact that in the trinomial analysis part of the net-capture probability $P_{\rm net}^{T\to P}$ is distributed over unphysical higher-order capture channels, which correspond to the production of negative ions. The

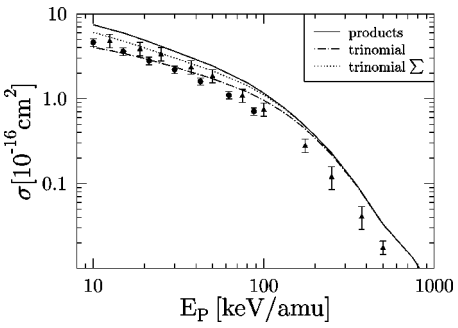

FIG. 3. Total cross section for neutralization of the projectile as a function of impact energy for $He^+ + Ne$ collisions. Theory: present calculations with time-dependent screening and analysis in terms of products of binomials (full curve) and trinomial analysis (chain curve). The dotted curve corresponds to a trinomial analysis, in which all contributions from single and multiple-capture events are added (without the corresponding multiplicities). Experiment: closed circles [10]; closed triangles [11].

included dotted curve shows that the capture cross section is increased considerably when these unphysical contributions are added. We note that norm conservation is maintained in the trinomial analysis only if these contributions are taken into account. Above $E_P = 100$ keV/amu both sets of calculations merge, since the contributions from multiple capture events decrease rapidly. Our results lie significantly above the experimental data in this region. At lower impact energies the agreement with experiment appears to be better for the trinomial analysis, but the shape of the products-of-binomials cross section curve reproduces the energy dependence of the experimental data.

In Sec. III B, we have argued that the Pauli exclusion principle would be important for capture processes. To assess its role we have applied the formalism of *inclusive probabilities*. The results are shown in Fig. 4. Due to the orthogonality problem discussed in Sec. III B these results may be flawed in particular at low impact energies and have to be interpreted with some caution. They are smaller than the results of the products-of-binomials analysis by an almost constant factor about 1.5–1.8, and are in remarkable agreement with experiment over the entire energy range. A close analysis of the single-particle solutions shows that the dominant capture process is the transition of a $Ne(2p_1)$ electron to the K shell of the projectile. The inclusive analysis ensures that this transition is blocked in the case of parallel spin directions, if the projectile electron remains in its ground state. We have checked that we obtain very similar results in a naive model for Pauli blocking, in which half of the single-particle probabilities for capture to the K shell is subtracted before applying the analysis in terms of products of binomials. Also included in Fig. 4 is the sum of single and higher-order capture obtained in the inclusive analysis. Obviously, multiple capture is considerably suppressed compared to the trinomial results displayed in Fig. 3. Note that the cross sections for the production of negative ions are nonzero in the inclusive analysis, since multiple capture to excited states is not blocked by the Pauli principle.

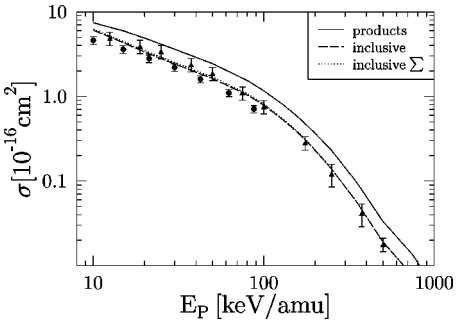

FIG. 4. Total cross section for neutralization of the projectile as a function of impact energy for $He^+ + Ne$ collisions. Theory: present calculations with time-dependent screening and analysis in terms of products of binomials (full curve) and inclusive analysis (broken curve). The dotted curve corresponds to an inclusive analysis, in which all contributions from single and multiple-capture events are added (without the corresponding multiplicities). Experiment: closed circles [10]; closed triangles [11].

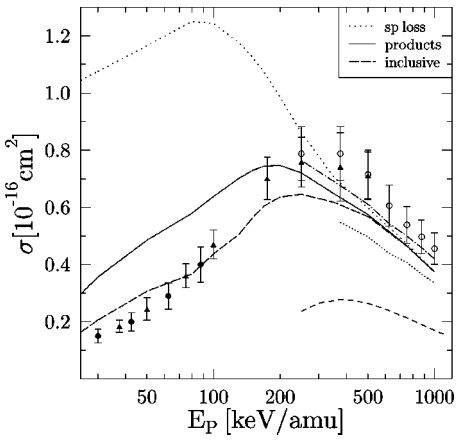

FIG. 5. Total cross section for electron loss from the projectile as a function of impact energy for $He^+ + Ne$ collisions. Theory: present calculations with time-dependent screening and analysis in terms of products of binomials (full curve) and inclusive analysis (broken curve). The dotted curve (sp loss) corresponds to the result of the single-particle calculation for the active He^+ electron; chain curve [9], dotted curve [16], short-dashed curve: PWBA calculation for the antiscreening mode [9]. Experiment: closed circles [10]; closed triangles [11]; open circles [12].

The inclusive analysis does not change the net capture probability $P_{\rm net}^{T\to P}$ and the average number of electrons on the projectile $P_{\rm av}^P$ [Eq. (35)] [18]. A reduction of the probability to find two electrons at the projectile P_2^P implies an increase of the probability to detect one bound electron P_1^P, as $P_{\rm av}^P \approx P_1^P + 2P_2^P$ when higher-order capture is neglected. This in turn results in a reduction of the probability to find no electron bound to the projectile P_0^P, as all probabilities must add to unity ($\Sigma_{k=0} P_k^P = 1$). As a consequence, the antisymmetry of the total wave function reduces the cross section for total electron loss, where the projectile is fully stripped. This is demonstrated in Fig. 5. The results of the inclusive analysis are smaller than the products-of-binomials cross sections except at high energies, where capture processes become unlikely. They are in very good agreement with the experimen-

tal data below the threshold for the electron-electron process (cf. Sec. IV A) and show that the interplay of capture and electron-loss processes is of crucial importance for this channel. However, they are also affected by the nonorthogonality problem discussed above. As an indication of this flaw we found, e.g., negative values for P_0^P in particular at energies $E_P \leqslant 50$ keV/amu and at impact parameters $b \geqslant 1.5$ a.u. In these cases we set $P_0^P = 0$ for the cross section calculation, thus introducing a sharp cutoff for the contributing impact-parameter range. At present we can only speculate how the electron loss cross section would decrease for lower impact energies in a calculation, which does not suffer from the nonorthogonality problem.

In addition to the inclusive and products-of-binomials results we have included in Fig. 5 the cross section obtained from a direct integration of the single-particle electron loss probability ($p^{P\to T+C} = p^{P\to T} + p^{P\to C}$) [Eqs. (32) and (33)] over impact parameter b. Except for high-impact energies this cross section is significantly larger than the other two, which demonstrates that the stripping of the projectile cannot be understood by considering the active projectile electron alone in this region. We note that a competition of electron loss and capture was also found at higher energies for C^{3+} and O^{5+}-ions colliding with noble gas atoms [13].

Also shown in Fig. 5 are the theoretical results of Refs. [9,16], which rely on similar effective single-particle equations for the active projectile electron as the one defined by the Hamiltonian (16) (see the discussion in Ref. [16]). In Ref. [9] the single-particle equation is solved in a projectile-centered basis, while the authors of Ref. [16] have used the sudden approximation, which involves the omission of energy phases. It is considered to be less accurate than the coupled-channel method, which was provided as an explanation for the discrepancies between both calculations [16]. Why the coupled-channel results of Ref. [9] are at variance with our single-particle electron loss cross section is unclear at present.

In addition, we have included the PWBA result for electron loss in the antiscreening mode [7,9] in Fig. 5. When this cross section is added to our products-of-binomials or inclusive cross section the sum lies slightly above the experimental error bars. However, as pointed out in Ref. [9] both cross sections should not be simply added, but the impact-parameter dependent probabilities have to be combined statistically to ensure that either of the processes takes place. This procedure resulted in a 7–12 % reduction compared to the simple sum in Ref. [9] and would lead to an acceptable agreement between theory and experiment in our case.

C. Charge-state correlated cross sections

An application of the inclusive analysis to charge-state correlated processes requires the construction of the single-particle density matrix with respect to bound states on both centers. Due to the artificial nature of the target s states and the absence of bound $l \neq 0$ states in the calculation of electron capture from the projectile [cf. Eq. (32)] we have not attempted to carry out this analysis. Instead, the following results are solely obtained from the analysis in terms of products of binomials. Given that Pauli blocking is crucial for electron capture, we do not discuss coincident data for capture and simultaneous target ionization.

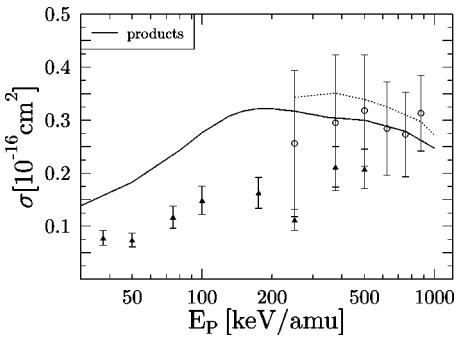

FIG. 6. Total cross section for elastic electron loss from the projectile as a function of impact energy for $He^+ + Ne$ collisions. Theory: present calculation with time-dependent screening and analysis in terms of products of binomials (full curve); dotted curve [15]. Experiment: closed triangles [11]; open circles [12,34], combined as described in [15].

Figure 6 shows the so-called elastic electron loss cross section, which corresponds to a fully stripped projectile ion and a neutral target atom after the collision. The electron-electron process is negligible for this cross section, since no target electrons are ionized. Electron loss by electron-electron interaction can only contribute if the active target electron is excited, but this process is rather unlikely [2]. Our results are in good agreement with the experimental data and the theoretical calculations reported in Ref. [15], but lie above the measurements of Ref. [11]. According to Fig. 5 we expect that our cross section would be reduced for low to intermediate impact energies in the inclusive analysis, but it is not possible to estimate this reduction quantitatively at present. We note that both sets of experimental data were not measured directly, but were obtained by forming the difference between the sum of all electron loss cross sections obtained in coincidence with the production of recoil ions and the separately measured total electron loss cross section.

The coincidence data are displayed in Fig. 7. The electron-electron process may contribute to all the cross sections shown, but the relative contributions for the different recoil ion charge states $q = 1 \cdots 4$ are not known. From the comparison between the experimental data and our calculations one can conclude that this process should contribute for $q = 1$ and $q = 2$, as our results are in very good agreement with the measurements below the threshold of this process ($E_{ts} \approx 140$ keV/amu, as discussed in Sec. IV A), but lie noticeably below them for higher-impact energies. Our calculations show good agreement with the experimental results for $q = 3$ at $E_P \geqslant 200$ keV/amu, but lie above them at lower-impact energies and significantly overestimate the $q = 4$ data over the entire energy range. We have found similar results for multiple ionization in bare-ion impact collisions [19,21]. At present it remains an open question, whether a more refined time-dependent screening model would reduce the cross sections for higher recoil ion charge states sufficiently, or whether the discrepancy can only be resolved by going beyond the IPM picture. Thus, we cannot estimate the im-

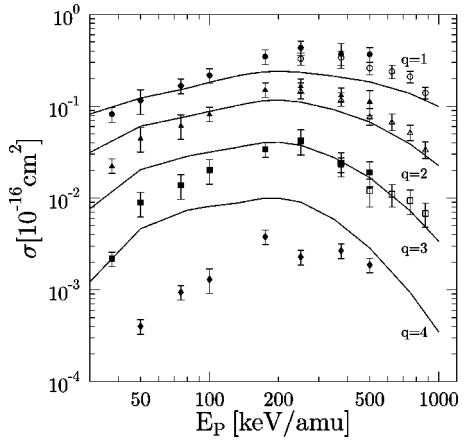

FIG. 7. Total cross section for electron loss from the projectile in coincidence with the production of a recoil ion in charge state q as a function of impact energy for $He^+ + Ne$ collisions. Theory: present calculation with time-dependent screening and analysis in terms of products of binomials. Experiment: closed symbols [11]; open symbols [34].

portance of the electron-electron process for $q=3,4$.

Finally, we present results for pure multiple-target ionization in Fig. 8. Given that the projectile does not change its charge state in this case antiscreening is of minor importance. It could contribute to multiple ionization by rather complicated processes, in which, e.g., one target electron and the projectile electron are both ionized due to the electron-electron interaction, and one target electron is captured to balance the final charge state of the projectile. Obviously, such processes are very unlikely, as the capture probabilities decrease rapidly at energies higher than the threshold of the electron-electron process.

Again, one observes in Fig. 8 that our results lie above the experimental data for $q=3$ and $q=4$. For the lower recoil ion charge states we find good agreement except for single ionization below $E_P=100$ keV/amu. In this region our cross sections are smaller than the experimental data. As time-dependent screening effects are of minor importance for

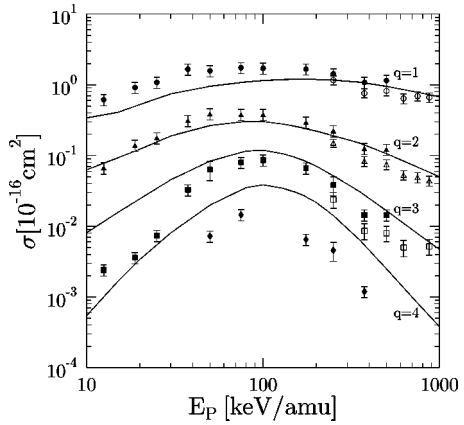

FIG. 8. Total cross section for pure multiple-target ionization corresponding to the recoil ion charge state q as a function of impact energy for $He^+ + Ne$ collisions. Theory: present calculation with time-dependent screening and analysis in terms of products of binomials. Experiment: closed symbols [11]; open symbols [34].

single-electron transitions it is unlikely that a more refined dynamical screening model would improve the agreement. To provide a possible explanation for the discrepancy we return to the inclusive analysis for the capture and loss channels described in the discussion of Figs. 4 and 5. We noted then that the reduction of the probability to find two electrons at the projectile P_2^P implies an increase in the probability P_1^P. This probability corresponds to the sum of all processes, in which the projectile does not change its charge state, i.e., elastic collisions and the pure multiple-ionization channels. Hence, the inclusive analysis could lead to an increased single (and multiple) ionization cross section at low to intermediate-impact energies. However, it is not possible to estimate the effects of this analysis on the individual multiple-ionization cross sections. From the reduction in P_2^P (Fig. 5) we can only conclude that the corresponding increase in P_1^P might be sufficient to explain the experimental cross section for single ionization. If this guess turns out to be correct it will imply an impressive inter-relation between the different inelastic processes in the nonperturbative regime.

V. CONCLUDING REMARKS

We have studied $He^+ + Ne$ collisions in the energy range 10 to 1000 keV/amu in the framework of the independent particle model (IPM). For the active target electrons we have included a dynamical screening potential that models the increasing attraction of the total target potential as ionization and capture set in. Repercussions of this effect on the propagation of the projectile electron, as well as time-dependent screening of the total projectile potential experienced by the target electrons are neglected. The reported results are obtained from the nonperturbative basis generator method, and statistical and *inclusive probability* analyses were carried out for *all* electrons.

We have found good overall agreement with experiment for a large number of rearrangement channels. This demonstrates that many aspects of a collision system that involves active electrons on both centers can be explained with sufficient accuracy on the basis of a rather simple model. For the total free-electron production and the projectile electron loss cross sections the agreement with the experimental data is improved when our results are combined with PWBA data for the electron-electron process (antiscreening), which is neglected in an IPM description.

Furthermore, we demonstrated the importance of the Pauli principle for electron capture to the projectile. Our results indicated that the antisymmetry of the total $(N+1)$-electron wave function may also affect the electron loss and target-ionization channels. A more detailed analysis of these effects in terms of *inclusive probabilities* was hampered by the problem that the time-propagated single-particle states of the target electrons are not orthogonal to the time-propagated projectile state in our approximation. This problem was found to be most prominent at low-impact energies. One can expect that a more refined dynamical screening model, in which all effective potentials due to the electron-electron in-

teraction are varied in time on an equal footing would alleviate this flaw.

In particular, the inclusion of dynamical screening in the Hartree potential v_H^T, which shields the nuclear target potential in Eq. (16) would result in a total effective target potential that exhibits a Coulomb tail and accommodates an infinite number of bound states in contrast to the exponentially decaying potential of the present *no-response* approximation [Eq. (16)]. As a consequence, electron transfer from the projectile to the target would be enhanced in such a model, which could explain the discrepancies with experiment found for our total recoil ion production cross section σ_+ at low-impact energies. Moreover, provided that the overlaps of the time-propagated orbitals are sufficiently small, an inclusive analysis could be carried out for all charge-state correlated cross sections, thus accounting for the Pauli exclusion principle on both centers in a consistent way.

The most sophisticated level of a refined dynamical screening model is the full TDHF problem of Eqs. (2) and (3), in which the nonorthogonality problem is not present. However, the solution of the TDHF equations is an extremely difficult and computationally costly task for the $He^+ + Ne$ collision system due to the coupling of the single-particle equations for the projectile and target electrons throughout the propagation. We reiterate that even global time-dependent screening models for all effective potentials result in a significant technical complication due to this coupling. Nevertheless, such an extension of our model seems feasible and will be addressed in a future work.

ACKNOWLEDGMENTS

We thank Eduardo Montenegro for very helpful discussions and the communication of the unpublished experimental data of Ref. [34], and Hans Jürgen Lüdde for a long-standing collaboration. This work has been supported by the Natural Sciences and Engineering Research Council of Canada. T.K. gratefully acknowledges financial support of the DAAD.

[1] E. C. Montenegro, W. E. Meyerhof, and J. H. McGuire, Adv. At., Mol., Opt. Phys. **34**, 249 (1994).
[2] C. L. Cocke and E. C. Montenegro, Comments At. Mol. Phys. **32**, 131 (1996).
[3] J. H. McGuire, *Electron Correlation Dynamics in Atomic Collisions* (Cambridge University Press, Cambridge, England, 1997), Chap. 8.
[4] H. -P. Hülskötter, W. E. Meyerhof, E. Dillard, and N. Guardala, Phys. Rev. Lett. **63**, 1938 (1989); H. -P. Hülskötter *et al.*, Phys. Rev. A **44**, 1712 (1991); E. C. Montenegro, W. S. Melo, W. E. Meyerhof, and A. G. de Pinho, Phys. Rev. Lett. **69**, 3033 (1992).
[5] R. Dörner *et al.*, Phys. Rev. Lett. **72**, 3166 (1994); W. Wu *et al.*, *ibid.* **72**, 3170 (1994); Phys. Rev. A **55**, 2771 (1997).
[6] D. R. Bates and G. Griffing, Proc. Phys. Soc., London, Sect. A **66**, 961 (1953); **67**, 663 (1954); **68**, 90 (1955).
[7] E. C. Montenegro and W. E. Meyerhof, Phys. Rev. A **43**, 2289 (1991).
[8] E. C. Montenegro and T. J. M. Zouros, Phys. Rev. A **50**, 3186 (1994).
[9] P. L. Grande, G. Schiwietz, G. M. Sigaud, and E. C. Montenegro, Phys. Rev. A **54**, 2983 (1996).
[10] M. E. Rudd, T. V. Goffe, A. Itoh, and R. D. DuBois, Phys. Rev. A **32**, 829 (1985).
[11] R. D. DuBois, Phys. Rev. A **39**, 4440 (1989).
[12] M. M. Sant'Anna, W. S. Melo, A. C. F. Santos, G. M. Sigaud, and E. C. Montenegro, Nucl. Instrum. Methods Phys. Res. B **99**, 46 (1995).
[13] W. S. Melo, M. M. Sant'Anna, A. C. F. Santos, G. M. Sigaud, and E. C. Montenegro, Phys. Rev. A **60**, 1124 (1999).
[14] K. Riesselmann, L. W. Anderson, L. Durand, and C. J. Anderson, Phys. Rev. A **43**, 5934 (1991).
[15] A. B. Voitkiv, G. M. Sigaud, and E. C. Montenegro, Phys. Rev. A **59**, 2794 (1999).
[16] A. B. Voitkiv, N. Grün, and W. Scheid, J. Phys. B **33**, 3431 (2000).
[17] T. Kirchner, L. Gulyás, H. J. Lüdde, A. Henne, E. Engel, and R. M. Dreizler, Phys. Rev. Lett. **79**, 1658 (1997).
[18] T. Kirchner, L. Gulyás, H. J. Lüdde, E. Engel, and R. M. Dreizler, Phys. Rev. A **58**, 2063 (1998).
[19] T. Kirchner, H. J. Lüdde, and R. M. Dreizler, Phys. Rev. A **61**, 012705 (2000).
[20] T. Kirchner, H. J. Lüdde, M. Horbatsch, and R. M. Dreizler, Phys. Rev. A **61**, 052710 (2000).
[21] T. Kirchner, M. Horbatsch, H. J. Lüdde, and R. M. Dreizler, Phys. Rev. A **62**, 042704 (2000).
[22] H. J. Lüdde, A. Henne, T. Kirchner, and R. M. Dreizler, J. Phys. B **29**, 4423 (1996).
[23] O. J. Kroneisen, H. J. Lüdde, T. Kirchner, and R. M. Dreizler, J. Phys. A **32**, 2141 (1999).
[24] A. Henne, A. Toepfer, H. J. Lüdde, and R. M. Dreizler, J. Phys. B **19**, L361 (1986).
[25] J. -P. Blaizot and G. Ripka, *Quantum Theory of Finite Systems* (MIT Press, Cambridge, 1986), Chap. 9; P. Ring and P. Schuck, *The Nuclear Many-Body Problem* (Springer, New York, 1980), Chap. 12.
[26] J. D. Talman and W. F. Shadwick, Phys. Rev. A **14**, 36 (1976); E. Engel and S. H. Vosko, *ibid.* **47**, 2800 (1993); E. Engel and R. M. Dreizler, J. Comput. Chem. **20**, 31 (1999).
[27] W. Stich, H. J. Lüdde, and R. M. Dreizler, Phys. Lett. **99A**, 41 (1983); K. Gramlich, N. Grün, and W. Scheid, J. Phys. B **19**, 1457 (1986).
[28] T. Kirchner, Ph.D. thesis, Universität Frankfurt, 1999.
[29] H. J. Lüdde and R. M. Dreizler, J. Phys. B **18**, 107 (1985).
[30] M. Horbatsch, Phys. Lett. A **187**, 185 (1994).
[31] P. Kürpick, H. J. Lüdde, W. D. Sepp, and B. Fricke, Z. Phys. D: At., Mol. Clusters **25**, 17 (1992).
[32] R. Anholt, Phys. Lett. A **114**, 126 (1986).
[33] A. A. Radzig and B. M. Smirnov, *Reference Data on Atoms, Molecules, and Ions*, Springer Series in Chemical Physics Vol. 31 (Springer, Berlin, 1985).
[34] A. C. F. Santos, Doctor of Science thesis, PUC-Rio, 1998; A. C. F. Santos, W. S. Melo, M. M. Sant'Anna, G. M. Sigaud, and E. C. Montenegro, Phys. Rev. A (to be published).